
ENHANCED DIAGNOSTIC PERFORMANCE VIA LARGE-RESOLUTION INFERENCE OPTIMIZATION FOR PATHOLOGY FOUNDATION MODELS

Mengxuan Hu*
University of Virginia
Charlottesville, VA, USA
qtq7su@virginia.edu

Zihan Guan*†
University of Virginia
Charlottesville, VA, USA
bxv6gs@virginia.edu

John Kang
Merck & Co., Inc.
Biometrics Research
Rahway, NJ, USA
jia.kang@merck.com

Sheng Li‡
University of Virginia
Charlottesville, VA, USA
shengli@virginia.edu

Zhongliang Zhou‡
Merck & Co., Inc.
Biometrics Research
Rahway, NJ, USA
zhongliang.zhou@merck.com

ABSTRACT

Despite their prominent performance on tasks such as ROI classification and segmentation, many pathology foundation models remain constrained by a specific input size e.g. 224×224 , creating substantial inefficiencies when applied to whole-slide images (WSIs), which span thousands of resolutions. A naïve strategy is to either enlarge inputs or downsample the WSIs. However, enlarging inputs results in prohibitive GPU memory consumption, while downsampling alters the microns-per-pixel resolution and obscures critical morphological details. To overcome these limitations, we propose an space- and time- efficient inference strategy that sparsifies attention using spatially aware neighboring blocks and filters out non-informative tokens through global attention scores. This design substantially reduces GPU memory and runtime during high-resolution WSI inference while preserving and even improving the downstream performance, enabling inference at higher resolutions under the same GPU budget. The experimental results show that our method can achieves up to an 7.67% improvement in the ROI classification and compatible results in segmentation.

Keywords Computational pathology · Foundation models · Inference Optimization

1 Introduction

Tissue analysis is vital for cancer diagnosis and treatment, and traditional glass slides are increasingly being replaced by digital whole-slide images (WSIs). This shift enables computational pathology to move into routine clinical use [1, 2, 3]. Recent advances are driven by foundation models [4, 5, 6]—large deep neural networks trained on massive datasets with self-supervised learning. These models generate versatile data embeddings that generalize across diverse tasks including ROI-level classification, segmentation, and image retrieval, offering a clear advantage over diagnostic-specific methods limited by smaller, less varied pathology datasets.

Despite their strong performance, most pathology foundation models—commonly built on Vision Transformer (ViT) architectures with the DINO algorithm, typically trained for a specific input size 224×224 or 448×448 . Whole-slide images (WSIs), however, contain information across thousands of resolutions, creating a substantial mismatch. A straightforward approach would be to either feed larger images directly into the model (since in principle Transformers

*Equal Contributions. † Zihan Guan performed the work during the internship at Biometrics Research, Merck & Co., Inc., Rahway, NJ, USA. ‡ Corresponding Authors.

can accept variable-length inputs) or to downsample them to match the trained input size. Both strategies inevitably introduce drawbacks. The former leads to quartic scaling of GPU memory usage and computation time with image resolution, while the latter alters the microns-per-pixel (mpp) resolution, potentially obscuring critical morphological features such as cellular atypia [4]. As shown in the right of Figure 1, the GPU memory quadratically increases in the vanilla inference mode.

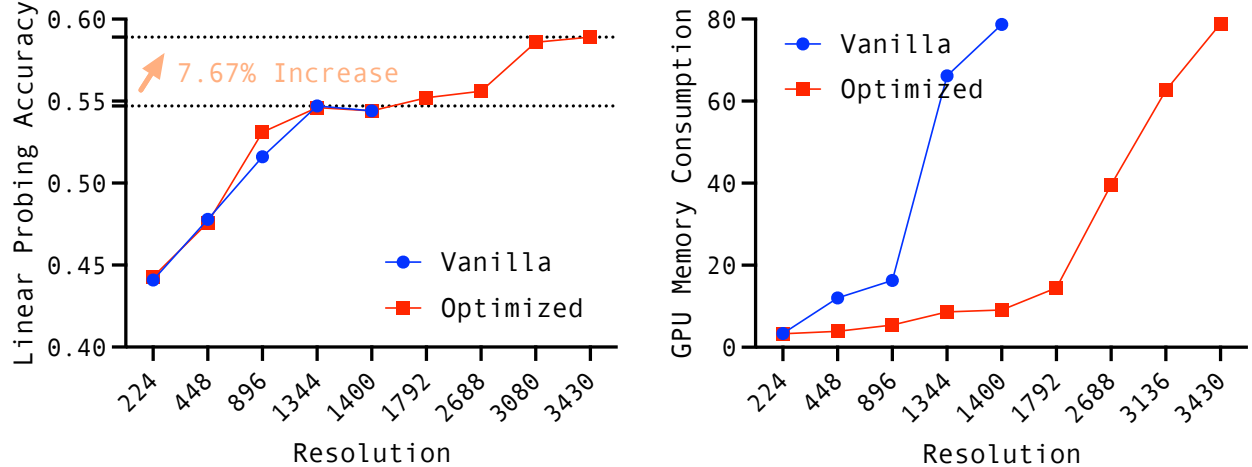


Figure 1: The left figure shows the interplay between the resolution and the linear probing accuracy on the PANDA dataset; The right figure shows the interplay between the resolution and the GPU memory consumption.

Our experimental results show that higher image resolutions generally lead to better downstream performance. Hence, we abandon the second solution and focus on improving the first one—feeding larger images directly into the model—by reducing GPU memory usage and runtime while maintaining or even improving performance. Specifically, we sparsify the attention matrix using spatially aware neighboring blocks, motivated by the observation that a cell’s most relevant signals and interactions are typically concentrated within its immediate microenvironment. In addition, to further accelerate inference, we leverage global attention scores to rank image tokens and filter out those corresponding to histologically non-informative regions—such as empty background, or tissue preparation artifacts. This reduces computational overhead while simultaneously removing noisy signals that can hinder performance. Our empirical experiments indicate that the combined approach not only achieves a significant GPU memory reduction and efficiency improvement, but also achieves 7.67% improvement in the classification task and compatible performance in the segmentation task.

To sum up, the contributions in this paper include:

- **Resolution and Performance:** The first paper that explicitly discusses the interplay between input resolution and the downstream performance of pathology foundation models.
- **Inference Optimization:** The first paper that focuses on optimizing the inference of the pathology foundation models.
- **Promising Performance:** We achieve significant reduction in GPU memory and improvement in efficiency.

2 Related Works

2.1 Digital Pathology Foundation Models

Foundational vision models have significantly advanced digital pathology analysis. Notable examples include CTransPath [7], which integrates convolutions within Transformers for spatial context; UNI [4], which uses hierarchical Transformers for multi-resolution processing; and GigaPath [5], which trains on gigapixel-scale images to capture fine-grained details. More recently, Virchow [6] was introduced as a pathology-specific foundation model that excels at capturing clinically relevant features from diverse histopathology data. These models are predominantly trained with ViTs or similar architectures, whose computational cost scales quartically with image size. This severely limits their direct application to WSIs.

2.2 Vision Transformers Inference Optimization

Pioneering studies on optimizing vision transformer inference for high-resolution images can be broadly categorized into two approaches. The first focuses on optimizing memory consumption within attention modules, as seen in methods like SparseAttention [8], FlashAttention [9], and vLLM [10]. The second approach aims to reduce computational overhead by pruning redundant attention calculations, exemplified by FastV [11] and FastGen [12]. Although these optimizations have been shown to reduce model overhead without sacrificing performance in other settings, their design for histopathology images remains underexplored. To our knowledge, this is the first paper to specifically address inference optimization for pathology foundation models. Furthermore, our method is the first to simultaneously combine both memory optimization and computational pruning techniques, creating a more comprehensive solution than the previous work.

3 Methodology

We first introduce the intuitions for the inference optimizations in Section 3.1. Then, introduce the optimization strategies for both memory efficiency and time efficiency in Section 3.2 and Section 3.3. The overall optimization mechanism is depicted in Figure 2.

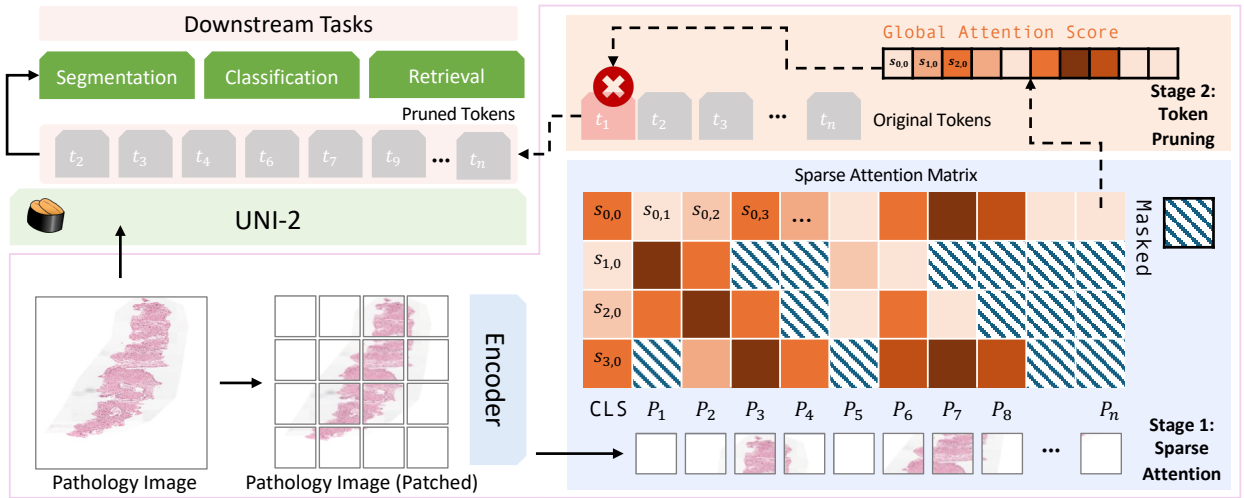


Figure 2: An overview of our inference optimization strategies. Sparse attention masks attention scores from distant tokens, while token pruning removes tokens with the lowest global attention scores.

3.1 The Trade-offs of Higher Resolutions

Higher resolutions generally leads to better performance. Taken UNI-2 model as an example, when we increase the resolution of the input images, the performance on the downstream classification task progressively increases (shown in the Figure 1 Left). However, the benefits come at a significant cost of memory consumption: The GPU memory consumption increases quartically along with the resolution (Right). Given the great potential benefits of using larger resolutions as inputs and the bottlenecks posed by the GPU memory consumption, it is natural to conjecture that, *can we push the Pareto frontier of the performance and the GPU memory consumption by optimizing the model inference process?*

3.2 Memory-Efficiency Optimization

The primary computational bottleneck is the quadratic memory complexity ($\mathcal{O}(N^2)$) of the self-attention mechanism, where the attention matrix multiplications can consume significant amount of GPU memories. This is further exemplified in ViT, as N itself scales quadratically with input resolution. To alleviate the memory burden, our approach is motivated by the observation that in histopathology images, a patch's most informative context lies within its immediate microenvironment. The inherent heterogeneity of tissue organization makes local neighborhoods particularly relevant for interpretation, whereas distant regions often contribute little. Conventional attention mechanisms, however, still allocate substantial computation to these less informative areas.

Therefore, we employ a sparse attention mechanism, inspired by BigBird [8]. Instead of computing the full attention matrix $A \in \mathbb{R}^{N \times N}$, where N is the number of tokens, we sparsify the interactions using a hybrid approach:

- **Local Windowed Attention:** Each token attends only to tokens corresponding to its spatially adjacent patches in the original pixel space. This efficiently captures high-fidelity local features and context.
- **Global Attention:** A few designated "global" tokens (e.g., CLS) attend to all other tokens in the sequence. This ensures that critical long-range dependencies are maintained across the entire image.

This combined strategy allows the model to build a rich understanding of the input by focusing computational resources on meaningful local interactions while still preserving essential global context.

3.3 Time-Efficiency Optimization

Our second optimization targets time efficiency. Even with sparse attention, the sequence length N can be very large for high-resolution images, leading to slow processing speeds. To accelerate computation, we introduce a dynamic token pruning stage, motivated by FastViT [11]. This method identifies and removes computationally redundant tokens—such as those corresponding to empty background regions or tissue artifacts—based on their contribution. Specifically, we derive an importance score for each of the N tokens from the global attention weights, forming a score vector $a \in \mathbb{R}^N$. We then rank all tokens by their importance and permanently discard a proportion p (where $0 \leq p < 1$) with the lowest scores. To ensure the scores contain meaningful semantic information before pruning, we apply the pruning after several initial layers have processed the data (e.g., after the fourth layer). This strategy dynamically shortens the sequence length for all subsequent layers, substantially reducing overall computation time. Furthermore, by pruning uninformative tokens, the model focuses more effectively on semantically relevant regions, leading to improved downstream performance.

4 Experimental Results

4.1 Experimental Setups

Tasks and Datasets We evaluate our method on two typical tasks for pathology foundation models: PANDA [13] dataset for cancer pattern classification and SegPath [14] for cancer histology segmentation. Detailed descriptions of the task setups are provided in the following sections.

Settings For all the experiments, the default window size is 8, and the pruning ratio is 0.6 unless otherwise specified. We adopt UNI-2 [4] as the backbone foundation model. However, the methodology can be easily integrated with other foundation models [5, 4, 15]. We manually resize the input images to simulate different image resolutions (e.g., 224, 448). All the experiments are conducted on an A100 (80GB) GPU.

4.2 Cancer Classification Task

Setup. The PANDA dataset is used for the task of classifying cancer tissue samples into one of five International Society of Urological Pathology (ISUP) scores. Following [4], we adopt two evaluation strategies when using pathology foundation models for this task: linear probing and K-Nearest Neighbor (KNN). Linear probing involves training a simple linear classifier on top of features extracted from the frozen, pre-trained foundation model. In contrast, KNN assigns a label to a test sample based on the majority vote of its 20 nearest neighbors in the feature space, using Euclidean distance. For both strategies, we report accuracy, the weighted F1-score, and the Area Under the Receiver Operating Characteristic curve (AUROC).

Main Results. Table 1 gives a full comparison of the performance, time efficiency, and GPU memory consumption between the vanilla inference workflow and our optimized method. As shown, when input with the same fixed resolution, our method significantly reduces time and GPU memory consumption while maintaining or even achieving better performance. The benefits in performance gain can be partially explained by our design of the inference strategy: the spatial-aware sparse attention largely maintains the necessary information for decision-making, and the pruned uninformative tokens guide the model to better capture the semantic information of the input images. Moreover, it is observed that on the standard A100 GPU of 80 GB GPU memory, our method eventually can accommodate inputs with 3430 resolutions, while the vanilla inference can accommodate inputs with only 1400 resolutions. This increase in input resolutions finally led to a significant increase in performance and efficiency in image processing for the real-world workflow.

Resolution	Method	Linear Probing			Time	
		Accuracy	Weighted F1	AUROC	Time	Memory
224	Vanilla	0.441	0.433	0.751	2,241	3.35
	Ours	0.443	0.436	0.750	2,181	3.32
448	Vanilla	0.478	0.474	0.777	2,248	12.03
	Ours	0.476	0.469	0.776	2,285	3.90
896	Vanilla	0.516	0.510	0.798	6,583	16.32
	Ours	0.531	0.522	0.816	3,476	5.41
1344	Vanilla	0.547	0.540	0.828	21,703	66.18
	Ours	0.546	0.538	0.832	7,668	8.66
1400	Vanilla	0.544	0.536	0.822	24,818	78.73
	Ours	0.544	0.534	0.830	8,360	9.12
1792	Vanilla	-	-	-	-	-
	Ours	0.552	0.545	0.841	13,588	14.50
2688	Vanilla	-	-	-	-	-
	Ours	0.556	0.545	0.843	30,315	39.61
3136	Vanilla	-	-	-	-	-
	Ours	0.586	0.576	0.849	41,368	62.63
3430	Vanilla	-	-	-	-	-
	Ours	0.589	0.574	0.852	89,640	78.87

Table 1: Performance comparison between our method and the vanilla UNI-2 model on the classification task. *Shorter* runtime and *lower* GPU usage are highlighted in green. *Longer* runtime and *higher* GPU usage are highlighted in red.

	Linear Probing			KNN		
	Accuracy	F1	AUROC	Accuracy	Bal. Acc.	F1
$p = 0.4$	0.576	0.569	0.852	0.479	0.415	0.463
$p = 0.5$	0.581	0.572	0.849	0.476	0.408	0.457
$p = 0.6$	0.586	0.576	0.849	0.480	0.411	0.461
$p = 0.7$	0.578	0.568	0.850	0.486	0.416	0.467
$p = 0.8$	0.572	0.562	0.849	0.473	0.402	0.452

Table 2: Ablation studies on pruning ratio p

	Linear Probing			KNN		
	Accuracy	F1	AUROC	Accuracy	Bal. Acc.	F1
$w = 2$	0.585	0.577	0.849	0.465	0.396	0.444
$w = 8$	0.586	0.576	0.849	0.480	0.411	0.461
$w = 16$	0.579	0.569	0.849	0.477	0.408	0.458
$w = 64$	0.573	0.561	0.849	0.463	0.400	0.443

Table 3: Ablation studies on windows size w

Ablation Studies. Table 2 and Table 3 present ablation studies on the pruning ratio p and window size w , respectively, when the image size is of resolution 3134 (i.e., 224×14). The results indicate that performance remains consistently stable across different choices of p and w .

Qualitative Examples on Image Token Pruning. Figure 3a visualizes the sparsified attention matrix. Figure 3b shows the pruned image tokens mapped back to the original pixel space, where the red rectangle  indicates a pruned image token. The pruning mainly results from empty background patches or less informative regions.

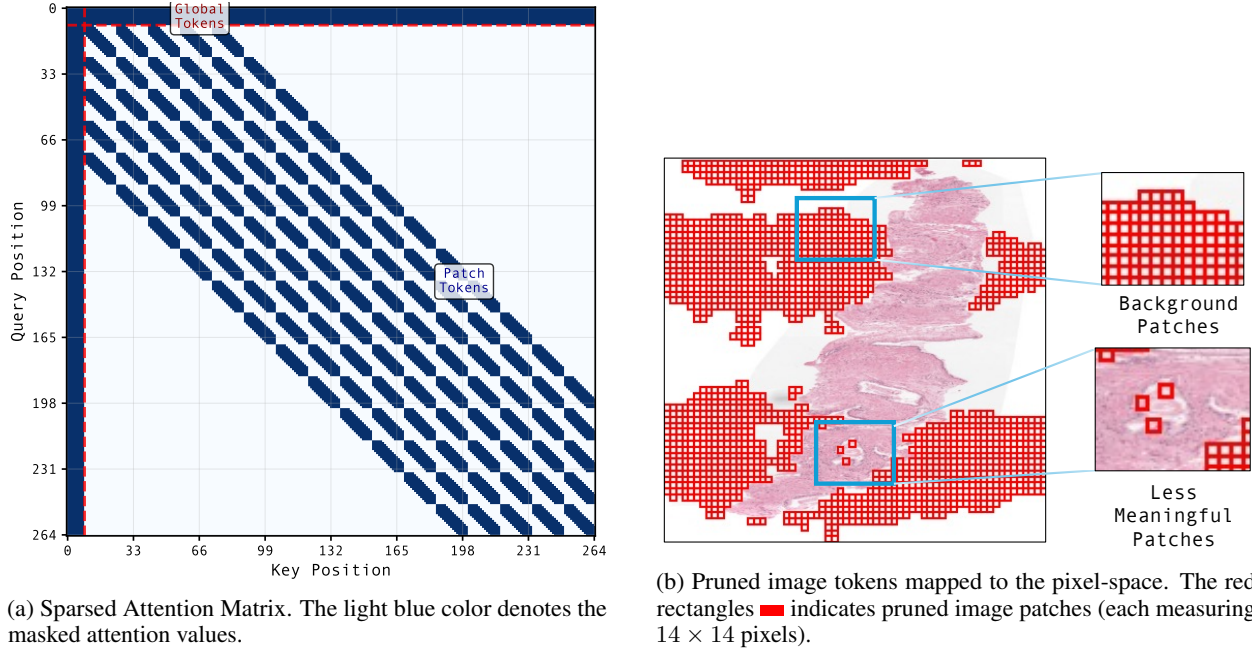


Figure 3: Qualitative examples of the sparse attention matrix and pruned image tokens.

4.3 Segmentation Task

Setup. SegPath is used for the tasks of segmenting eight major cell types in tumor tissue: epithelial cells, smooth muscle cells, red blood cells, endothelial cells, leukocytes, lymphocytes, plasma cells, and myeloid cells. Each image is of size 984×984 . We employ the Mask2Former model [16], fine-tuned with a Vision Transformer Adapter (ViT-Adapter) to segment eight major cell types within tumor tissues using the SegPath dataset. The training hyperparameters follow the setups in [17]. Following the prior work [4, 17, 18], we report metrics such as Mean Pixel Accuracy (MPA), class pixel accuracy (CPA), Intersection over Union (IoU), and Dice, using the averaged performance across the eight cell types in the SegPath. It is noted that Mask2Former requires feature maps that preserve the original image’s spatial structure; we cannot apply the time-efficiency optimization described in Section 3.3 to the features extracted by the UNI-2 model. Therefore, we do not report the time consumption in the Table 4.

Main Results The results for the segmentation task show a similar pattern as in the classification task (see Table 4). However, since segmentation relies on global spatial information, sparsifying the attention matrix inevitably drops semantical information that is potentially meaningful to the segmentation. Therefore, the performance gap between our method and the vanilla method is relatively larger.

Ablation Studies Table 5 presents the ablation studies on the window size c , when the image size is of resolution 560. The results indicate that the performance tends to improve when the window size is larger, which aligns with the intuition that the segmentation task relies more on the global features.

Qualitative Examples on Segmentation Performance Figure 4 presents the qualitative examples of the UNI-2’s performance on the segmentation task when the input pixel varies from 112×112 to 448×448 . As shown, the predicted segmentation mask aligns more precisely with the ground-truth segmentation mask when the resolution increases.

5 Conclusion and Future Directions

In this paper, we propose an inference optimization method for digital pathology foundation models. The results on ROI classification and segmentation tasks demonstrate the effectiveness of our method. Despite the promising performance, there are still many directions to explore, e.g., What other methods could be specially designed for the vision language model (VLM)-based pathology foundation models?

Resolution	Method	Segmentation Performance			Memory
		MPA	IoU	Dice	
112	Vanilla	0.632	0.553	0.657	7.15
	Ours	0.642	0.458	0.587	6.93
224	Vanilla	0.727	0.553	0.678	12.99
	Ours	0.661	0.467	0.596	12.77
336	Vanilla	0.742	0.517	0.650	24.09
	Ours	0.678	0.497	0.623	22.79
448	Vanilla	0.749	0.579	0.702	42.33
	Ours	0.709	0.565	0.686	35.38
560	Vanilla	0.743	0.568	0.701	60.03
	Ours	0.709	0.558	0.678	52.55

Table 4: Performance comparison between our method and the vanilla UNI-2 model on the segmentation task. *Lower* GPU usage is highlighted in **green**. *Higher* GPU usage is highlighted in **red**.

	MPA	IoU	Dice
$w = 2$	0.686	0.547	0.66
$w = 8$	0.709	0.558	0.678
$w = 16$	0.710	0.559	0.680
$w = 64$	0.723	0.576	0.696

Table 5: Ablation studies on windows size w .

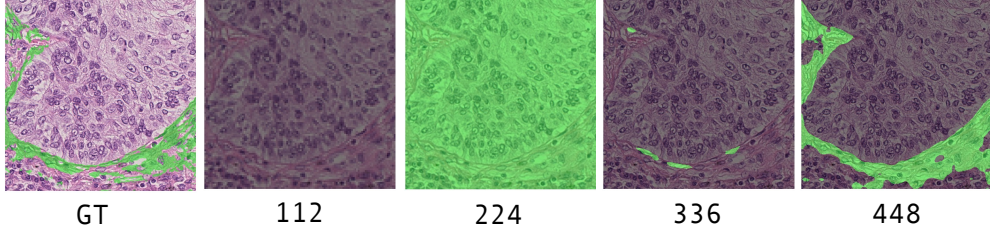


Figure 4: Qualitative examples of the UNI-2’s performance on the segmentation task when the input pixel varies.

Acknowledgments

This project is supported by Merck BARDS Academic Collaboration Grant.

References

- [1] Zihan Guan, Hanyin Wang, Zhongliang Zhou, Qiaohui Zhou, Peining Tao, and Junshui Ma. Pharmadata-agent: A specialized agent for pharmaceutical data analysis. In *The Second Workshop on GenAI for Health: Potential, Trust, and Policy Compliance*, 2025.
- [2] Zihan Guan, Zihao Wu, Zhengliang Liu, Dufan Wu, Hui Ren, Quanzheng Li, Xiang Li, and Ninghao Liu. Cohortgpt: An enhanced gpt for participant recruitment in clinical study. *arXiv preprint arXiv:2307.11346*, 2023.
- [3] Zhengliang Liu, Zihao Wu, Mengxuan Hu, Bokai Zhao, Lin Zhao, Tianyi Zhang, Haixing Dai, Xianyan Chen, Ye Shen, Sheng Li, et al. Pharmacygpt: The ai pharmacist. *arXiv preprint arXiv:2307.10432*, 2023.
- [4] Richard J Chen, Tong Ding, Ming Y Lu, Drew FK Williamson, Guillaume Jaume, Andrew H Song, Bowen Chen, Andrew Zhang, Daniel Shao, Muhammad Shaban, et al. Towards a general-purpose foundation model for computational pathology. *Nature Medicine*, 30(3):850–862, 2024.
- [5] Hanwen Xu, Naoto Usuyama, Jaspreet Bagga, Sheng Zhang, Rajesh Rao, Tristan Naumann, Cliff Wong, Zelalem Gero, Javier González, Yu Gu, et al. A whole-slide foundation model for digital pathology from real-world data. *Nature*, 630(8015):181–188, 2024.

- [6] Eugene Vorontsov, Alican Bozkurt, Adam Casson, George Shaikovski, Michal Zelechowski, Siqi Liu, Kristen Severson, Eric Zimmermann, James Hall, Neil Tenenholz, et al. Virchow: A million-slide digital pathology foundation model. *arXiv preprint arXiv:2309.07778*, 2023.
- [7] Xiyue Wang, Sen Yang, Jun Zhang, Minghui Wang, Jing Zhang, Wei Yang, Junzhou Huang, and Xiao Han. Transformer-based unsupervised contrastive learning for histopathological image classification. *Medical image analysis*, 81:102559, 2022.
- [8] Manzil Zaheer, Guru Guruganesh, Kumar Avinava Dubey, Joshua Ainslie, Chris Alberti, Santiago Ontanon, Philip Pham, Anirudh Ravula, Qifan Wang, Li Yang, et al. Big bird: Transformers for longer sequences. *Advances in neural information processing systems*, 33:17283–17297, 2020.
- [9] Tri Dao, Dan Fu, Stefano Ermon, Atri Rudra, and Christopher Ré. Flashattention: Fast and memory-efficient exact attention with io-awareness. *Advances in neural information processing systems*, 35:16344–16359, 2022.
- [10] Woosuk Kwon, Zhuohan Li, Siyuan Zhuang, Ying Sheng, Lianmin Zheng, Cody Hao Yu, Joseph E. Gonzalez, Hao Zhang, and Ion Stoica. Efficient memory management for large language model serving with pagedattention. In *Proceedings of the ACM SIGOPS 29th Symposium on Operating Systems Principles*, 2023.
- [11] Liang Chen, Haozhe Zhao, Tianyu Liu, Shuai Bai, Junyang Lin, Chang Zhou, and Baobao Chang. An image is worth 1/2 tokens after layer 2: Plug-and-play inference acceleration for large vision-language models, 2024.
- [12] Suyu Ge, Yunan Zhang, Liyuan Liu, Minjia Zhang, Jiawei Han, and Jianfeng Gao. Model tells you what to discard: Adaptive KV cache compression for LLMs. In *The Twelfth International Conference on Learning Representations*, 2024.
- [13] Wouter Bulten, Kimmo Kartasalo, Po-Hsuan Cameron Chen, Peter Ström, Hans Pinckaers, Kunal Nagpal, Yuannan Cai, David F Steiner, Hester Van Boven, Robert Vink, et al. Artificial intelligence for diagnosis and gleason grading of prostate cancer: the panda challenge. *Nature medicine*, 28(1):154–163, 2022.
- [14] Daisuke Komura, Takumi Onoyama, Koki Shinbo, Hiroto Odaka, Minako Hayakawa, Mieko Ochi, Ranny Rahang-ingrum Herdiantoputri, Haruya Endo, Hiroto Katoh, Tohru Ikeda, et al. Restaining-based annotation for cancer histology segmentation to overcome annotation-related limitations among pathologists. *Patterns*, 4(2), 2023.
- [15] Ming Y Lu, Bowen Chen, Drew FK Williamson, Richard J Chen, Ivy Liang, Tong Ding, Guillaume Jaume, Igor Odintsov, Long Phi Le, Georg Gerber, et al. A visual-language foundation model for computational pathology. *Nature Medicine*, 30(3):863–874, 2024.
- [16] Bowen Cheng, Ishan Misra, Alexander G Schwing, Alexander Kirillov, and Rohit Girdhar. Masked-attention mask transformer for universal image segmentation. In *Proceedings of the IEEE/CVF conference on computer vision and pattern recognition*, pages 1290–1299, 2022.
- [17] Fang Yan, Jianfeng Wu, Jiawen Li, Wei Wang, Jiaxuan Lu, Wen Chen, Zizhao Gao, Jianan Li, Hong Yan, Jiabo Ma, et al. Pathorchestra: A comprehensive foundation model for computational pathology with over 100 diverse clinical-grade tasks. *arXiv preprint arXiv:2503.24345*, 2025.
- [18] Zihan Guan, Mengxuan Hu, Zhongliang Zhou, Jielu Zhang, Sheng Li, and Ninghao Liu. Badsam: Exploring security vulnerabilities of sam via backdoor attacks (student abstract). In *Proceedings of the AAAI Conference on Artificial Intelligence*, volume 38, pages 23506–23507, 2024.